NASA TECHNICAL MEMORANDUM

NASA TM X-71467

NASA TM X-71467

THREE-DIMENSIONAL ELASTIC STRESS AND DISPLACEMENT ANALYSIS OF FINITE GEOMETRY SOLIDS CONTAINING CRACKS

by John P. Gyekenyesi and Alexander Mendelson
Lewis Research Center
Cleveland, Ohio 44135

TECHNICAL PAPER proposed for presentation at
Seventh U.S. National Congress of Applied Mechanics sponsored
by the U.S. National Committee of Theoretical and Applied
Mechanics of the National Academy of Sciences
Boulder, Colorado, June 3-7, 1974

THREE-DIMENSIONAL ELASTIC STRESS AND DISPLACEMENT ANALYSIS OF FINITE GEOMETRY SOLIDS CONTAINING CRACKS*

by John P. Gyekenyesi and Alexander Mendelson
Lewis Research Center

SUMMARY

The line method of analysis is applied to the Navier-Cauchy equations of elastic equilibrium to calculate the displacement distributions in various bodies containing cracks. The application of this method to these equations leads to coupled sets of simultaneous ordinary differential equations whose solutions are obtained along sets of lines in a discretized region. When decoupling the equations and their boundary conditions is not possible, the use of a successive approximation procedure permits the analytical solution of the resulting ordinary differential equations. The results obtained show a considerable potential for using this method in the three-dimensional analysis of finite geometry solids and suggest a possible extension of this technique to nonlinear material behavior.

E-7170

INTRODUCTION

Considerable progress has been made in recent years in the stress analysis of bodies containing flaws or cracks. However, most of the work on this subject has been based on the plane theory of elasticity (ref. 1). For a fracture specimen of finite geometry the stress and displacement fields are highly three-dimensional. Hence, solutions of the general elasticity

---

* Submitted to the International Journal of Fracture Mechanics.

field equations must be obtained when more reliable results are needed.

Because of the geometric singularity associated with any crack type problem, there is almost no possibility of a simple closed form type of solution. For this reason, three-dimensional elastic solutions have been obtained only for a restricted class of problems (refs. 2 to 4). Recently, with the availability of large digital computers, a variety of numerical methods appeared in the literature; however, most of these methods have yielded only partial results. Among these approximate methods are the finite difference (ref. 5), the finite element (ref. 6), the direct potential (ref. 7), the eigenfunction expansion (ref. 8), and the line method of analysis (refs. 9 to 11). Of all these solution techniques, the line method of analysis appears to yield the most complete and accurate results for three-dimensional elasticity problems.

Although the concept of the line method for solving partial differential equations is not new (ref. 12), its application in the past has been limited to simple examples (ref. 13). The line method lies midway between completely analytical and discrete methods. The basis of this technique is the substitution of finite differences for the derivatives with respect to all the independent variables except one for which the derivatives are retained. This approach replaces a given partial differential equation with a system of simultaneous ordinary differential equations whose solutions can then be obtained in closed form. These equations describe the dependent variable along lines which are parallel to the coordinate in whose direction the deriv-

atives were retained. Application of the line method is most useful when the resulting ordinary differential equations are linear and have constant coefficients.

An inherent advantage of the line method over other numerical methods is that good results are obtained from the use of relatively coarse grids. This use of a coarse grid is permissible because parts of the solutions are obtained in terms of continuous functions. Additional accuracy in normal stress distributions is derived from the fact that they are expressed as first-order derivatives of the displacements and these derivatives can be analytically evaluated. Inherently inaccurate numerical differentiation is required only for evaluating the shear stresses, but this presents no important loss of accuracy since they are an order of magnitude smaller than the normal stresses. For problems with geometric singularities, additional accuracy is derived from using a displacement formulation since the resulting deformations are not singular.

It is the purpose of this report to present a simple and systematic approach to the elastic analysis of three-dimensional, finite geometry solids containing traction-free cracks. The need for these specific solutions has existed for a number of years in fracture toughness testing. Problems that are most conveniently described in rectangular Cartesian coordinates as well as circular geometry solids are treated.

REDUCTION OF THE NAVIER-CAUCHY EQUATIONS TO SYSTEMS OF ORDINARY DIFFERENTIAL EQUATIONS

Within the framework of linearized elasticity theory, the equations of elastic equilibrium in terms of displacements are

$$(\lambda + G)\frac{\partial e}{\partial x} + G\nabla^2 u = 0 \tag{1}$$

$$(\lambda + G)\frac{\partial e}{\partial y} + G\nabla^2 v = 0 \tag{2}$$

$$(\lambda + G)\frac{\partial e}{\partial z} + G\nabla^2 w = 0 \tag{3}$$

where the body forces are assumed to be zero and the dilatation is

$$e = \frac{\partial u}{\partial x} + \frac{\partial v}{\partial y} + \frac{\partial w}{\partial z} \tag{4}$$

For a finite geometry solid with rectangular boundaries, we construct three sets of parallel lines (fig. 1(a)). Each set of lines is parallel to one of the coordinate axes and thus perpendicular to the corresponding coordinate plane. An approximate solution of equation (1) can then be obtained by developing solutions of ordinary differential equations along the x-directional lines. As seen in the figure, there are a total of ℓ = NY x NZ such lines where NY is the number of lines along the y-direction and NZ is the number of lines along the z-direction in a given plane, respectively. We define the displacements along these lines as $u_1, u_2, \ldots, u_\ell$. The derivatives of the y-directional displacements on these lines with respect to y are defined as $v'|_1, v'|_2, \ldots, v'|_\ell$, and the derivatives of the z-directional displacements

with respect to z are defined as $w'|_1$, $w'|_2$, . . . , $w'|_\ell$. These displacements and derivatives can then be regarded as functions of x only since they are variables on x-directional lines. When these definitions are used, the ordinary differential equation along a generic line ij (a double subscript is used here for simplicity of writing) in figure 1(b) may be written as

$$\frac{d^2u_{ij}}{dx^2} + \frac{(1 - 2\nu)}{2(1 - \nu)}\left[-\left(\frac{2}{h_y^2} + \frac{2}{h_z^2}\right)u_{ij} + \frac{1}{h_y^2}(u_{i+1,j} + u_{i-1,j}) + \frac{1}{h_z^2}(u_{i,j+1} + u_{i,j-1})\right] + \frac{f_{ij}(x)}{2(1 - \nu)} = 0 \qquad (5)$$

where

$$f_{ij}(x) = \left.\frac{dv'}{dx}\right|_{ij} + \left.\frac{dw'}{dx}\right|_{ij} \qquad (6)$$

$$v' = \frac{dv}{dy}$$

and

$$w' = \frac{dw}{dz}$$

Similar differential equations are obtained along the other x-directional lines. Since each equation has the terms of the displacements on the surrounding lines, these equations constitute a system of ordinary differential equations for the displacements u_1, u_2, . . . , u_ℓ.

The set of ℓ second order differential equations represented by (5) can be reduced to a set of 2ℓ first order differential equations by treating

the derivatives of the u's as an additional set of ℓ unknowns, i.e. defining

$$u_{\ell+1} = \frac{du_1}{dx}, \; u_{\ell+2} = \frac{du_2}{dx}, \text{ etc.} \tag{7}$$

The resulting 2ℓ equations can now be written as a single first order matrix differential equation

$$\frac{dU}{dx} = A_1 U + R_1(x) \tag{8}$$

where U and R are column matrices of 2ℓ elements each and A_1 is a $2\ell x 2\ell$ matrix of the constant coefficients appearing in equations (5) and (7).

In a similar manner, to solve equations (2) and (3) ordinary differential equations are constructed along the y- and z-directional lines respectively. These equations are also expressed in an analogous form to equations (8); they are

$$\frac{dV}{dy} = A_2 V + S(y) \tag{9}$$

$$\frac{dW}{dz} = A_3 W + T(z) \tag{10}$$

Equations (8) to (10) are linear first-order ordinary matrix differential equations. They are, however, not independent, but are coupled through the vectors R, S and T whose components are given by equations similar to (6). The elements of the coefficient matrices A_1, A_2 and A_3 are all constants, being functions of the coordinate increments and Poisson's ratio only.

Noting that a second-order differential equation can satisfy only a total of two boundary conditions and since three-dimensional elasticity problems have three boundary conditions at every point of the bounding surface, some of the boundary data must be incorporated into the surface line differential equations. Hence, conditions of normal stress and displacement are enforced through the constants of the homogeneous solutions while shear stress boundary data must be incorporated into the differential equations of the surface lines. The application of the specified shear conditions permits the use of central difference approximations when surface line differential equations are constructed. The details of constructing these equations are found in reference 9.

EQUATIONS IN CYLINDRICAL COORDINATES

The Navier-Cauchy equations in cylindrical coordinates are written as

$$\left.\begin{aligned} \frac{\partial e}{\partial r} + (1 - 2\nu)\left[\left(\nabla^2 - \frac{1}{r^2}\right)u - \frac{2}{r^2}\frac{\partial v}{\partial \theta}\right] = 0 \\ \frac{1}{r}\frac{\partial e}{\partial \theta} + (1 - 2\nu)\left[\left(\nabla^2 - \frac{1}{r^2}\right)v + \frac{2}{r^2}\frac{\partial u}{\partial \theta}\right] = 0 \\ \frac{\partial e}{\partial z} + (1 - 2\nu)\nabla^2 w = 0 \end{aligned}\right\} \tag{11}$$

where the body forces are assumed to be zero and the dilatation is

$$e = \frac{\partial u}{\partial r} + \frac{1}{r}\frac{\partial v}{\partial \theta} + \frac{u}{r} + \frac{\partial w}{\partial z} \tag{12}$$

For a finite geometry body with circular boundaries, we construct

three sets of parallel lines in the direction of the coordinates as shown in figure 2. Approximate solutions of equations (11) can then be obtained by developing solutions of ordinary differential equations along the radial, circumferential, and axial lines, respectively. For the first of equations (11), we define the displacements along the radial lines as $u_1, u_2, \ldots, u_\ell$. The derivatives of the circumferential displacements on these lines with respect to θ are defined as $v'_1, v'_2, \ldots, v'_\ell$, and the derivatives of the axial displacements with respect to z are defined as $w'_1, w'_2, \ldots, w'_\ell$. These displacements and derivatives can then be regarded as functions of the radius only, since they are variables on radial lines. If these definitions are used, the ordinary differential equation along a generic, radial line ij of figure 2 may be written as

$$\left[\frac{d^2u_{ij}}{dr^2} + \frac{1}{r}\frac{du_{ij}}{dr} - \frac{u_{ij}}{r^2}\right] + \frac{(1 - 2\nu)}{2(1 - \nu)}\left[-\left(\frac{2}{r^2h_\theta^2} + \frac{2}{h_z^2}\right)u_{ij} + \frac{1}{r^2h_\theta^2}(u_{i+1,j} + u_{i-1,j}) + \frac{1}{h_z^2}(u_{i,j+1} + u_{i,j-1})\right] + \frac{f_{ij}(r)}{2(1 - \nu)} = 0 \qquad (13)$$

where

$$f_{ij}(r) = \frac{(4\nu - 3)}{r^2}\, v'\Big|_{ij} + \frac{1}{r}\frac{dv'}{dr}\Big|_{ij} + \frac{dw'}{dr}\Big|_{ij} \qquad (14)$$

and

$$v' = \frac{dv}{d\theta}$$

$$w' = \frac{dw}{dz}$$

Similar differential equations are obtained along the other radial lines. Since each equation has the terms of the displacements on the surrounding lines, these equations constitute a system of ordinary differential equations for the displacements $u_1, u_2, \ldots, u_\ell$.

Noting that a second-order differential equation can satisfy only a total of two boundary conditions, the shear stress boundary data must again be incorporated into the surface line differential equations. For the first radial line of figure 2, the use of zero shear stress boundary conditions in the radial direction on the r,z and r,θ coordinate planes gives, respectively, the following imaginary radial line displacements:

$$\left.\begin{aligned} u_{1\theta e} &= u_2 + 2h_\theta r \left.\frac{dv}{dr}\right|_1 - 2h_\theta v|_1 \\ u_{1\theta n} &= u_{N\theta+1} + 2h_z \left.\frac{dw}{dr}\right|_1 \end{aligned}\right\} \tag{15}$$

Equations (15) must then be used in the application of central difference approximations when the ordinary differential equation for the first radial line is generated. Additional details on the construction of these equations can be found in reference 9.

As before the system of ℓ second order equations given by equation (13) can be written as a single first order matrix equation

$$\frac{dU}{dr} = A_r(r)U + R(r) \tag{16}$$

where in this case the elements of U are defined by

$$\left.\begin{aligned} U_1 = ru_1,\ U_2 = ru_2, \ldots\ldots, U_\ell = ru_\ell \\ U_{\ell+1} = \frac{1}{r}\frac{d(ru_1)}{dr},\ U_{\ell+2} = \frac{1}{r}\frac{d(ru_2)}{dr}, \ldots, U_{2\ell} = \frac{1}{r}\frac{d(ru_\ell)}{dr} \end{aligned}\right\} \quad (17)$$

and the elements of the coefficient matrix $A_r(r)$ are no longer constant, but are functions of r. The corresponding equations for V and W are the same as (9) and (10) with y replaced by θ, the coefficient matrices being constant.

SOLUTION OF THE SYSTEMS OF ORDINARY DIFFERENTIAL EQUATIONS

The systems of ordinary differential equations (8) to (10) and (16) can be solved by any of a number of standard techniques. The method used herein was basically the matrizant or Peano-Baker method of integration (ref. 14). For equation (8) the solution can be written as

$$U(x) = e^{A_1 x} U(0) + e^{A_1 x} \int_0^x e^{-A_1 \eta} R(\eta) d\eta \quad (18)$$

with similar solutions for equations (9) and (10). U(0) is the initial value vector, determined from the boundary conditions. The conversion of given boundary data into required initial values is discussed in more detail in reference 9.

The matrizant $e^{A_1 x}$ is generally evaluated by its matrix series. For larger values of x, when convergence becomes slow, additive formulas may be used. In addition similarity transformations can be used to diagonalize the matrix A_1. These various techniques for improving the accuracy are discussed in detail in reference 9.

For the case of equation (16) the solution is more complicated, since we no longer have constant coefficients. The solution may be expressed as follows (ref. 14):

$$U(r) = \Omega(A_r)U(r_o) + \Omega(A_r)\int_{r_o}^{r}\left[\Omega(A_r)\right]^{-1} R(\eta)d\eta \qquad (19)$$

where r_o is the initial value of r which may or may not be zero. The matrizant $\Omega(A_r)$ is given by the infinite matrix integral series

$$\Omega(A_r) = I + \int_{r_o}^{r} A_r(\eta_1)d\eta_1 + \int_{r_o}^{r} A_r(\eta_2)d\eta_2 \int_{r_o}^{\eta_2} A_r(\eta_1)d\eta_1$$

$$+ \int_{r_o}^{r} A_r(\eta_3)d\eta_3 \int_{r_o}^{\eta_3} A_r(\eta_2)d\eta_2 \int_{r_o}^{\eta_2} A_r(\eta_1)d\eta_1 + \cdots \qquad (20)$$

which of course becomes very difficult to evaluate. However, by substituting the matrix A_r into equation (20), it can be seen by inspection, (ref. 9), that $\Omega(A_r)$ can be partitioned into four submatrices which satisfy the following equations:

$$\left.\begin{aligned} \frac{1}{r}\frac{d\Omega_{11}}{dr} &= \Omega_{21} \\ r\frac{d\Omega_{21}}{dr} &= \Omega_{11}K_r \\ \frac{1}{r}\frac{d\Omega_{12}}{dr} &= \Omega_{22} \\ r\frac{d\Omega_{22}}{dr} &= \Omega_{12}K_r \end{aligned}\right\} \qquad (21)$$

with

$$\Omega_{11}\Big|_{r=r_o} = \Omega_{22}\Big|_{r=r_o} = I$$

$$\Omega_{12}\Big|_{r=r_o} = \Omega_{21}\Big|_{r=r_o} = O$$

and K_r is the sub matrix of A_r obtained from the identity:

$$A_r = \begin{bmatrix} O & rI \\ \frac{1}{r}K_r & O \end{bmatrix}$$

Instead of evaluating the matrizant $\Omega(A_r)$ by means of equation (20), it can be evaluated by solving equations (21). This was done for the examples presented herein, using the single step Runge-Kutta integration method for solving equations (21).

Since equations (8) to (10) and their boundary conditions are highly coupled, it is generally impossible to directly evaluate their solutions. Thus, a successive approximation procedure must be employed where as-

sumed values must be used initially for the required unknowns. The cyclic resubstitution of the obtained solutions into the coupling vectors and the boundary conditions will usually converge to the correct solution, depending mainly on the accuracy to which the required matrizant can be evaluated.

Once the displacement field in the body has been calculated and the successive approximation procedure has converged, the normal stress distributions can be obtained directly by using the stress-displacement equations. The shear stresses, however, can be evaluated only through finite difference approximations for the required displacement gradients.

NUMERICAL RESULTS

Solid Cylindrical Bar with Penny-Shaped Crack

Figure 3 shows a cylindrical bar containing a penny-shaped crack and loaded by a uniform normal stress distribution. For problems with axisymmetric geometry, the circumferential displacement is inherently zero at every point and all the remaining variables are independent of the circumferential coordinate θ. The two sets of parallel lines needed for the solution of this problem are also shown in this figure. Note that the crack edge is assumed to be midway between adjacent nodes, specifying normal stress and displacement boundary conditions, respectively.

The solution of this problem was obtained by using two different sets of lines along the coordinate axes so that the convergence of the finite difference approximations could be checked. Selected results are shown in figures

4-6. Figure 4 shows that a relatively course grid of nine axial lines and nine radial lines gave almost identical results to those obtained using a 16 by 13 grid. Figures 5 and 6 compare the results obtained herein with analytical results of references 15 and 16 for infinite bodies and infinitely long finite radius cylinders with cracks. Both figures show that as the dimensions of the cylinder increase relative to the crack radius, the results from the method of lines approach the analytical results, as expected.

Table I shows the axial stress distribution for one case. The accuracy of the normal stress boundary conditions can be noted from the listed results.

Annular Plate with Internal Surface Cracks

A much more difficult problem of a thick annular plate with four symmetrically situated internal surface cracks and loaded by a uniform radial tensile load, is shown in figures 7 and 8. Because of symmetry only one-sixteenth of the orginal plate has to be discretized. Only a relatively coarse grid of 4 by 4 by 4 lines was used. Some of the results are shown in Tables 2 to 5.

Because of the use of a coarse grid, the numerical results for this example are somewhat inaccurate in magnitude but they do indicate some previously unknown variations in the stress field for this problem. This conclusion is possible in that the line method does not usually require a fine grid for good results as was shown in the previous section. These results also demonstrate that the method of lines permits the computation of the displacement and stress fields for a general three-dimensional problem.

APPLICATION TO TENSILE FRACTURE SPECIMENS CONTAINING CRACKS

A great amount of experimental work has been done in fracture mechanics (ref. 17) through the use of crack-notched specimens. In the past, many different types of specimens have been used to determine a material's fracture toughness. The most common early specimens employed in these tests were the center-cracked and double-edge-notched bar specimens. Figures 9(a) and 10(a) show the finite rectangular bars with through-thickness, traction-free central and double-edge cracks, respectively. Because of the symmetric geometry and loading, only one-eighth of the bars has to be discretized as shown in figures 9(b) and 10(b).

NUMERICAL RESULTS

Center-Cracked Tensile Fracture Specimen

The solution of this problem was obtained by using two different sets of lines along the coordinate axes so that the convergence of the finite difference approximations could be checked. In a given direction, uniform line spacing was used in all computations with no other restriction being placed on the selection of the grid size. The crack edge location with respect to the imposed grid was assumed to be halfway between nodes specifying normal stress and displacement boundary conditions, respectively. The successive approximation procedure required for decoupling the three sets of ordinary differential equations was terminated when the difference between successively calculated displacements at every point was less than a preset value (10^{-6}).

Selected results of the dimensionless displacements are listed in tables 6 to 8. The dimensionless crack opening displacement is shown in figure 11. Inspection of figures 11(a) and (b) shows that the grids of lines have been sufficiently refined when the results of the 64 by 112 by 112 grid were calculated. Figure 11(a) also contains the results of the plane elasticity solutions obtained by Mendelson, Gross, and Srawley (ref. 18). It is noteworthy that the results correspond to elliptical crack profiles in all cases. As can be noted from figure 11(c), the finite length of the bar has a very noticeable effect on the crack opening displacements for values of $L<3a$. Figure 11(d) shows the variation of the crack opening displacements across the thickness of the bar.

The dimensionless normal stress distributions in the crack plane are shown in figures 12 to 14 as a function of both the x- and z-coordinates. The results in these figures clearly indicate the singular nature of the normal stresses near the crack edge. As expected, the stress normal to the crack plane increases most rapidly near the crack front. A plot of these stresses in the z-direction also indicates a central region of uniform stress and a boundary layer through which the stresses decrease to the surface values. These same results show that as x increases the stress field approaches a uniaxial state of stress which indicates that the cause of a triaxial stress field in the bar is the through-thickness central crack.

Double-Edge Crack Tensile Fracture Specimen

The crack opening displacements for the problem of figure 10(a) are presented in figure 15. Comparing figures 15(a) and (b) shows that the finite difference approximations have sufficiently converged when the results of the finer grid were calculated. Contrary to the central crack problem, the crack opening displacements in figure 15 are independent of the z-coordinate. Similar results were obtained by Cruse and Van Buren (ref. 7) for the single-edge-crack bar specimen.

STRESS INTENSITY FACTOR

It is customary in fracture mechanics to describe the plane elasticity crack opening displacement as a superposition of three basic deformation modes (ref. 1). Since the problems shown in figures 9(a) and 10(a) have geometric symmetry and are symmetrically loaded, only the opening mode of crack displacement is obtained. In terms of the stress intensity factor for the opening mode K_I, the plane elasticity crack displacements near the crack tip are given by (ref. 1)

$$v\Big|_{y=0} = \frac{2(1-\nu)}{G} K_I \sqrt{\frac{R}{2\pi}} \qquad \text{plane strain} \tag{22}$$

$$v\Big|_{y=0} = \frac{2}{(1+\nu)G} K_I \sqrt{\frac{R}{2\pi}} \qquad \text{plane stress} \tag{23}$$

where R here is the distance from the crack edge. Since three-dimensional problems are neither in a state of plane strain nor in a state of plane stress, the definition of a stress intensity factor for these problems must

be first established. Note that by definition the plane stress and plane strain stress intensity factors are equal while the displacements are approximately 12.5 percent different for $\nu = 1/3$. Since the results indicate that for a sufficiently long bar most of the bar in the thickness direction is approximately in a state of plane strain, equation (22) is selected to calculate the stress intensity factor. Rearranging this equation so that the dimensionless crack opening displacements can be used leads to

$$\frac{E}{\sigma_o} C_I K_I = \frac{\left.\frac{Ev}{\sigma_o a}\right|_{y=0}}{\sqrt{\frac{R}{a}}} \tag{24}$$

where

$$C_I = \frac{4(1 - \nu^2)}{E\sqrt{2\pi a}}$$

A plot of equation (24) as $\sqrt{R/a} \to 0$ can then be used to calculate K_I. Since the crack opening displacement is a function of the thickness variable, the previously defined stress intensity factor varies in the z-direction. It should be noted that this description of K_I is completely arbitrary and that it is questionable if it has any real significance in three-dimensional elasticity problems. However, the values of K_I are presented here so that a comparison is possible with published plane strain solutions (ref. 1).

Figure 16 shows the variation across the thickness of the stress intensity factor for the center-cracked bar. Note that K_I is a maximum at the surface and a minimum near the center. The value of K_I for the double-edge-crack specimen is independent of the z coordinate since the crack opening displacement is constant across the thickness.

Although the stress intensity factors for these problems could be determined with reasonable accuracy, the associated type of singularities are difficult to evaluate because values of the normal stresses are needed within a distance of $0.05a$ or less from the crack edge. With the equal spacing of lines used in these examples, the minimum node location for these problems is about $0.06a$. For this range of crack edge distance R, the singularity of the stresses is not defined.

CONCLUSIONS

The line method of analysis presented affords a practical straight forward way for analysis of three-dimensional crack problems, at least for bodies with reasonably regular boundaries. Because parts of the solution are obtained as continuous functions along the lines chosen, relatively good accuracy can be obtained with coarse grids. In addition it should be noted that the introduction of plasticity into the analysis could be accomplished by merely changing the coupling terms appearing in equations (14) to (16). Since these have to be determined by an iterative process in any case, it would seem possible to solve the elastoplastic problem by a simple exten-

sion of the present method. Whether this approach is practical requires further investigation.

REFERENCES

1. Paris, Paul C.; and Sih, George C.: Stress Analysis of Cracks. Fracture Toughness Testing and Its Applications. Spec. Tech. Publ. No. 381, ASTM, 1965, pp. 30-83.

2. Sneddon, I.N.: The Distribution of Stress in the Neighborhood of a Crack in an Elastic Solid. Proc. Roy. Soc. (London), Ser. A, vol. 187, no. 1009, Oct. 22, 1946, pp. 229-260.

3. Smith, Frederick W.: Stresses Near a Semi-Circular Edge Crack. Ph.D. Thesis, Univ. of Washington, 1966.

4. Kassir, M.K.; and Sih, G.C.: Three-Dimensional Stress Distribution Around an Elliptical Crack Under Arbitrary Loadings. J. Appl. Mech., vol. 33, no. 3, Sept. 1966, pp. 601-611.

5. Ayres, David J.: A Numerical Procedure for Calculating Stress and Deformation Near a Slit in a Three-Dimensional Elastic-Plastic Solid. NASA TM X-52440, 1968.

6. Zienkiewicz, Olgierd C.: The Finite Element Method in Engineering Science. Second ed., McGraw-Hill Book Co., Inc., 1971.

7. Cruse, T.A.; and Van Buren, W.: Three-Dimensional Elastic Stress Analysis of a Fracture Specimen with an Edge Crack. Int. J. Fracture Mech., vol. 7, Mar. 1971, pp. 1-15.

8. Hartranft, R.J.; and Sih, G.C.: The Use of Eigenfunction Expansions in the General Solution of Three-Dimensional Crack Problems. J. Math. Mech., vol. 19, no. 2, Aug. 1969, pp. 123-138.

9. Gyekenyesi, John P.: Solution of Some Mixed Boundary Value Problems of Three-Dimensional Elasticity by the Method of Lines. Ph.D. Ph.D. Thesis, Michigan State Univ., 1972.

10. Gyekenyesi, John P.; Mendelson, Alexander; and Kring, Jon: Three-Dimenensional Elastic Stress and Displacement Analysis of Tensile Fracture Specimens Containing Cracks. NASA TN D-7213, 1973.

11. Gyekenyesi, John P.; Mendelson, Alexander; and Kring, Jon: Three-Dimensional Elastic Stress and Displacement Analysis of Finite Circular Geometry Solids Containing Cracks. NASA TN D-7266, 1973.

12. Faddeva, V.N.: The Method of Lines Applied to Some Boundary Problems. Trudy Mat. Inst. Steklov., vol. 28, 1949, pp. 73-103.

13. Irobe, Makoto: Method of Numerical Analysis for Three-Dimensional Elastic Problems. Proceedings of the 16th Japan National Congress for Applied Mechanics. Central Scientific Publ., 1968, pp. 1-7.

14. Frazer, R.A.; Duncan, W.J.; and Collar, A.R.: Elementary Matrices and Some Applications to Dynamics and Differential Equations. Cambride University Press, 1938.

15. Sneddon, I.N.: The Distribution of Stress in the Neighborhood of a Crack in an Elastic Solid. Proc. Roy. Soc. (London), Ser. A, vol. 187, no. 1009, Oct. 22, 1946, pp. 229-260.

16. Sneddon, I.N.; and Welch, J.T.: A Note on the Distribution of Stress in a Cylinder Containing a Penny-Shaped Crack. Int. J. Eng. Sci., vol. 1, 1963, pp. 411-419.

17. Brown, W.F., Jr.; and Srawley, J.E.: Plane Strain Crack Toughness Testing of High Strength Metallic Materials. Spec. Tech. Publ. No. 410, ASTM, 1967.

18. Mendelson, Alexander; Gross, Bernard; and Srawley, John E.: Evaluation of the Use of a Singularity Element in Finite-Element Analysis of Center-Cracked Plates. NASA TN D-6703, 1972.

TABLE 1. - NONDIMENSIONALIZED AXIAL STRESS σ_z/σ_o FOR SOLID CYLINDRICAL BAR WITH PENNY-SHAPED CRACK UNDER UNIFORM NORMAL TENSION

[a = 1.0, b = 1.77, L = 1.68 (16 axial and 13 radial lines).]

z	r								
	0.000	0.235	0.471	0.706	0.941	1.060	1.294	1.530	1.770
0.00	0.000	0.000	0.000	0.000	0.000	3.320	1.512	1.206	0.989
.28	.095	.093	.146	.319	.874	1.513	1.365	1.201	1.082
.56	.277	.295	.386	.592	.950	1.150	1.230	1.186	1.172
.84	.515	.542	.624	.770	.957	1.041	1.122	1.136	1.159
1.12	.736	.759	.808	.885	.972	1.010	1.059	1.082	1.092
1.40	.900	.915	.933	.960	.990	1.003	1.022	1.036	1.037
1.68	.999	.998	.999	.999	1.000	.999	.995	.993	.990

TABLE 2. - DIMENSIONLESS CIRCUMFERENTIAL DISPLACEMENTS $Ev/\sigma_o b$ FOR ANNULAR PLATE WITH INTERNAL SURFACE CRACKS UNDER UNIFORM RADIAL TENSION ON OUTSIDE SURFACE

z	θ, deg			
	0	15	30	45
r = 0.25				
0.00	0.718	0.566	0.302	0.000
.10	.592	.450	.238	↓
.20	.000	.073	.063	
.30	.000	.009	.012	
r = 0.50				
0.00	0.425	0.285	0.138	0.000
.10	.350	.232	.115	↓
.20	.000	.075	.057	
.30	.000	.023	.026	
r = 0.75				
0.00	0.000	0.037	0.029	0.000
.10	↓	.033	.026	↓
.20		.023	.020	
.30		.014	.014	
r = 1.00				
0.00	0.000	0.006	0.004	0.000
.10	↓	.007	.005	↓
.20		.009	.007	
.30		.010	.007	

TABLE 3. - DIMENSIONLESS RADIAL STRESS DISTRIBUTION σ_r/σ_o FOR ANNULAR PLATE WITH INTERNAL SURFACE CRACKS UNDER UNIFORM RADIAL TENSION ON OUTSIDE SURFACE

θ, deg	r			
	0.25	0.50	0.75	1.00
z = 0.00				
0	0.000	0.020	1.062	1.000
15	↓	.346	.837	↓
30		.293	.748	
45		.282	.726	
z = 0.10				
0	0.000	0.027	1.048	1.000
15	↓	.405	.872	↓
30		.424	.801	
45		.424	.783	
z = 0.20				
0	0.000	1.305	1.026	1.000
15	↓	.968	.980	↓
30		.840	.932	
45		.801	.915	
z = 0.30				
0	0.000	0.872	1.005	1.000
15	↓	.950	1.004	↓
30		.966	.986	
45		.956	.975	

TABLE 4. - DIMENSIONLESS CIRCUMFERENTIAL STRESS σ_θ/σ_o FOR ANNULAR PLATE WITH INTERNAL SURFACE CRACKS UNDER UNIFORM RADIAL TENSION ON OUTSIDE SURFACE

θ, deg	r			
	0.25	0.50	0.75	1.00
z = 0.00				
0	0.000	0.000	1.702	1.251
15	.308	.803	1.542	1.339
30	.209	1.043	1.460	1.416
45	.240	1.145	1.441	1.443
z = 0.10				
0	0.000	0.000	1.659	1.246
15	.703	.957	1.534	1.331
30	.803	1.196	1.472	1.410
45	.863	1.270	1.456	1.439
z = 0.20				
0	4.569	2.821	1.506	1.236
15	3.609	2.011	1.526	1.313
30	2.971	1.706	1.506	1.400
45	2.748	1.629	1.498	1.432
z = 0.30				
0	3.050	1.858	1.442	1.220
15	3.110	1.879	1.500	1.301
30	3.171	1.825	1.523	1.397
45	3.167	1.775	1.524	1.432

TABLE 5. - DIMENSIONLESS AXIAL STRESS σ_z/σ_o FOR ANNULAR PLATE WITH INTERNAL SURFACE CRACKS UNDER UNIFORM RADIAL TENSION ON OUTSIDE SURFACE

θ, deg	r			
	0.25	0.50	0.75	1.00
z = 0.00				
0	-1.974	-1.049	0.030	-0.014
15	-.939	-.126	.043	.040
30	-.631	.041	.064	.060
45	-.544	.082	.070	.062
z = 0.10				
0	-1.597	-1.073	0.028	-0.010
15	-.867	-.210	.032	.031
30	-.579	.006	.053	.046
45	-.487	.055	.059	.048
z = 0.20				
0	0.500	0.313	0.002	-0.004
15	-3.135	-1.996	-1.504	-1.310
30	-.077	.070	.039	.019
45	-.097	.073	.042	.020
z = 0.30				
0	0.000	0.000	0.000	0.000
15	↓	↓	↓	↓
30				
45				

TABLE 6. - DIMENSIONLESS x-DIRECTIONAL DISPLACEMENTS $Eu/\sigma_o a$ FOR RECTANGULAR BAR UNDER UNIFORM TENSION CONTAINING THROUGH-THICKNESS CENTRAL CRACK

[a = 1.0; b = 2.0; L = 1.75; t = 1.5 (64 by 112 by 112 x-, y-, z-directional lines, respectively).]

y	x						z
	0.00	0.31	0.77	1.23	1.69	2.00	
	x-Directional displacements, $Eu/\sigma_o a$						
0.00	0.00	-0.478	-1.047	-1.320	-1.391	-1.437	0.00
.50	↓	-.123	-.307	-.678	-.999	-1.103	↓
1.00		-.002	-.059	-.245	-.463	-.572	
1.75		.220	.447	.489	.404	.324	
0.00	0.00	-0.494	-1.084	-1.305	-1.331	-1.383	1.07
.50	↓	-.111	-.282	-.636	-.949	-1.061	↓
1.00		.011	-.034	-.213	-.431	-.546	
1.75		.241	.489	.534	.438	.350	
0.00	0.00	-0.410	-0.914	-1.196	-1.324	-1.340	1.50
.50	↓	-.043	-.153	-.556	-.934	-1.061	↓
1.00		.036	.013	-.183	-.424	-.546	
1.75		.238	.483	.525	.428	.338	

TABLE 7. - DIMENSIONLESS y-DIRECTIONAL DISPLACEMENTS $Ev/\sigma_o a$ FOR RECTANGULAR BAR UNDER UNIFORM TENSION CONTAINING THROUGH-THICKNESS CENTRAL CRACK

[a = 1.0; b = 2.0; L = 1.75; t = 1.5 (64 by 112 by 112 x-, y-, z-directional lines, respectively).]

z	y						x
	0.00	0.25	0.50	1.00	1.50	1.75	
	y-Directional displacements, $Ev/\sigma_o a$						
0.00	2.742	2.892	2.997	3.227	3.536	3.688	0.00
.43	2.769	2.912	3.018	3.246	3.556	3.708	
1.07	2.946	3.070	3.157	3.369	3.678	3.835	
1.50	3.258	3.343	3.397	3.569	3.871	4.034	
0.00	1.703	1.849	2.055	2.526	2.972	3.173	0.77
.43	1.718	1.863	2.069	2.542	2.988	3.189	
1.07	1.812	1.952	2.158	2.631	3.080	3.282	
1.50	1.974	2.088	2.283	2.752	3.205	3.410	
0.00	0.000	0.328	0.689	1.362	1.924	2.178	1.54
.43		.332	.695	1.371	1.932	2.186	
1.07		.348	.722	1.409	1.973	2.225	
1.50		.343	.722	1.432	2.007	2.257	
0.00	0.000	0.137	0.328	0.822	1.328	1.581	2.00
.43		.140	.333	.829	1.334	1.586	
1.07		.151	.353	.860	1.362	1.608	
1.50		.148	.353	.874	1.383	1.627	

TABLE 8. - DIMENSIONLESS z-DIRECTIONAL DISPLACEMENTS $Ew/\sigma_o a$ FOR RECTANGULAR BAR UNDER UNIFORM TENSION CONTAINING THROUGH-THICKNESS CENTRAL CRACK

[a = 1.0; b = 2.0; L = 1.75; t = 1.5 (64 by 112 by 112 x-, y-, z-directional lines, respectively).]

x	z						y
	0.00	0.43	0.64	1.07	1.28	1.50	
	z-Directional displacements, $Ew/\sigma_o a$						
0.00	0.00	0.036	0.068	0.185	0.272	0.366	0.0
.77	↓	-.055	-.081	-.123	-.124	-.095	↓
1.54		-.161	-.249	-.459	-.581	-.704	
2.00		-.179	-.270	-.441	-.512	-.568	
0.00	0.00	-0.042	-0.059	-0.077	-0.082	-0.090	0.5
.77	↓	-.097	-.147	-.247	-.296	-.342	↓
1.54		-.162	-.247	-.429	-.522	-.610	
2.00		-.176	-.264	-.430	-.505	-.574	
0.00	0.00	-0.123	-0.184	-0.307	-0.370	-0.435	1.0
.77	↓	-.144	-.217	-.366	-.442	-.517	↓
1.54		-.168	-.253	-.423	-.507	-.590	
2.00		-.176	-.262	-.425	-.501	-.577	
0.00	0.00	-0.222	-0.339	-0.595	-0.738	-0.886	1.75
.77	↓	-.212	-.320	-.546	-.662	-.780	↓
1.54		-.191	-.285	-.465	-.549	-.629	
2.00		-.190	-.281	-.446	-.521	-.593	

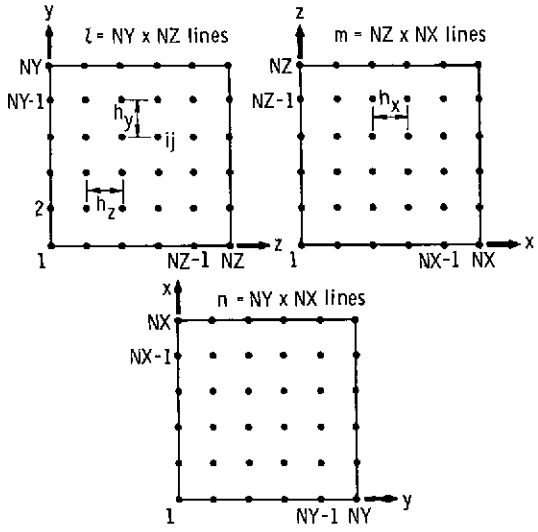

(a) Three sets of lines parallel to x-, y-, and z-coordinates and perpendicular to corresponding coordinate planes.

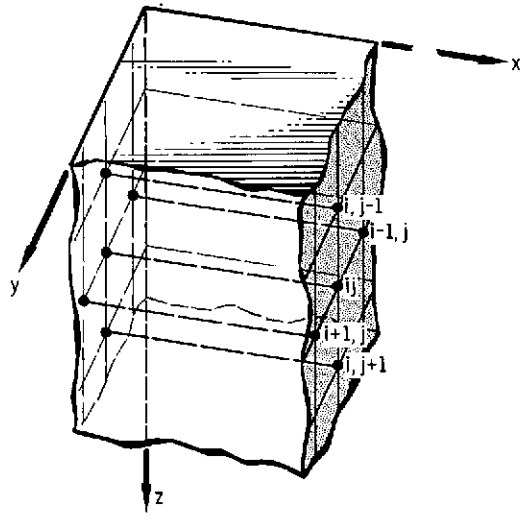

(b) Set of interior lines parallel to x-coordinate.

Figure 1. - Sets of lines parallel to Cartesian coordinates.

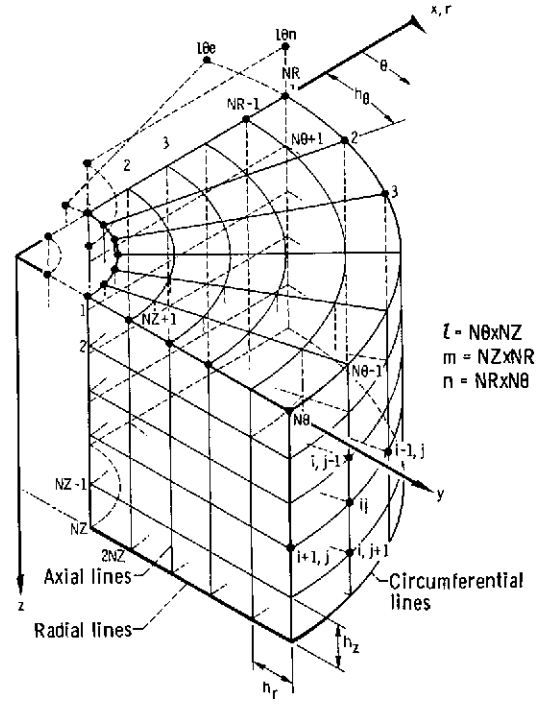

Figure 2. - Sets of lines is direction of cylindrical coordinates.

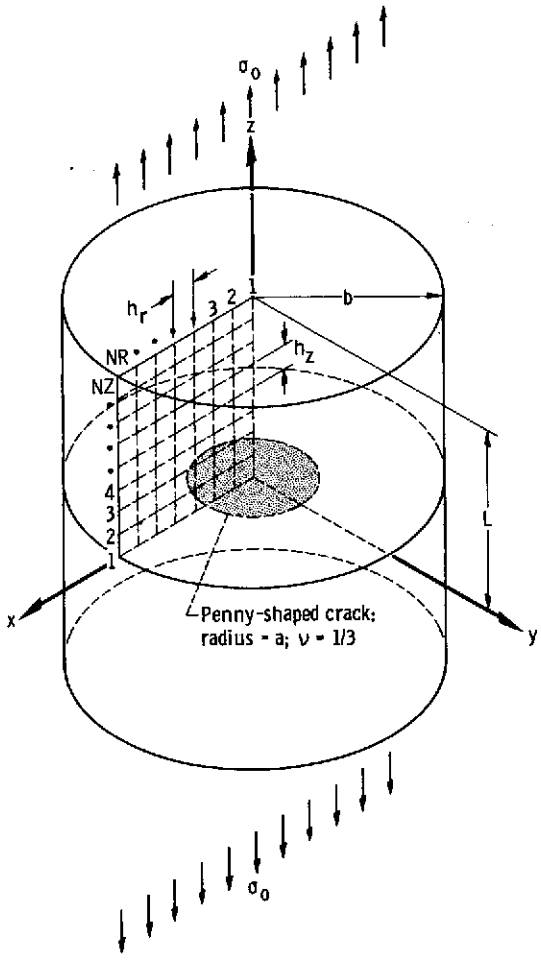

Figure 3. - Solid cylindrical bar with penny-shaped crack.

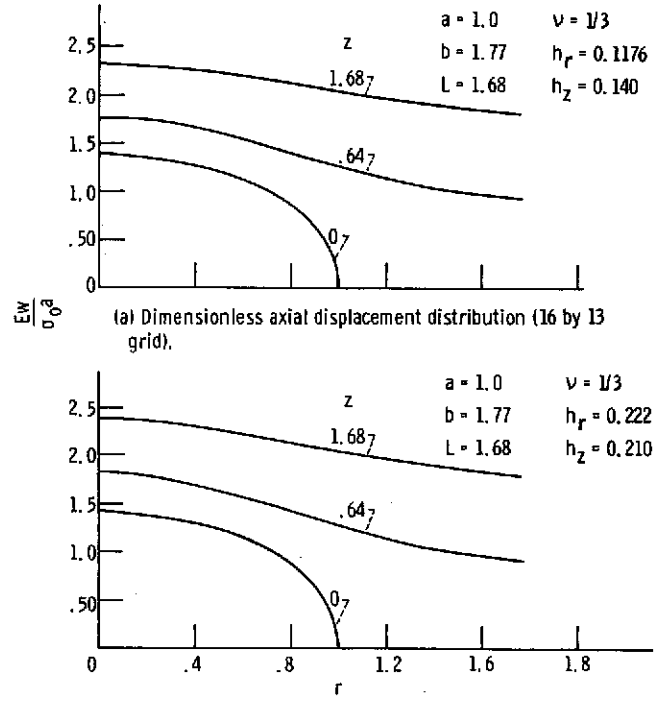

(a) Dimensionless axial displacement distribution (16 by 13 grid).

(b) Dimensionless axial displacement distribution (9 by 9 grid).

Figure 4. - Dimensionless axial displacement distribution for solid cylindrical bar with penny-shaped crack.

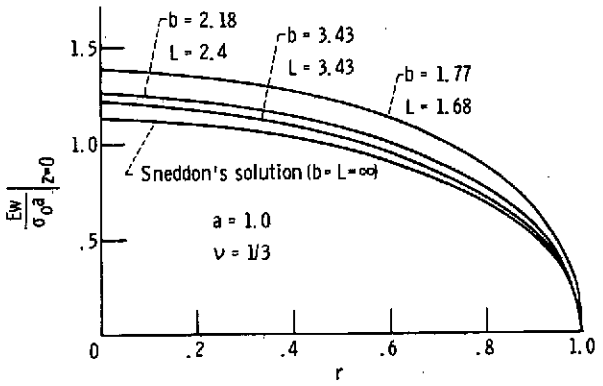

Figure 5. - Dimensionless crack opening displacements for solid cylindrical bars with penny-shaped cracks of various lengths and radii.

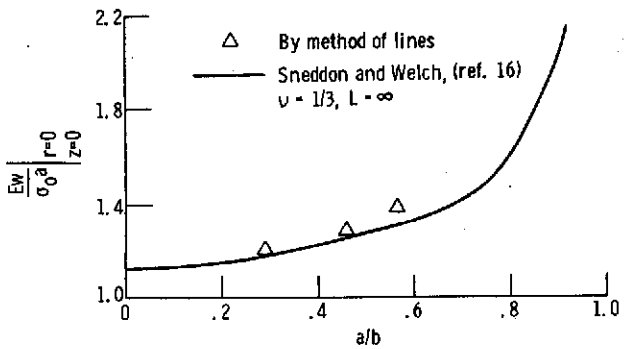

Figure 6. - Dimensionless maximum crack opening as function of crack to cylinder radius ratio.

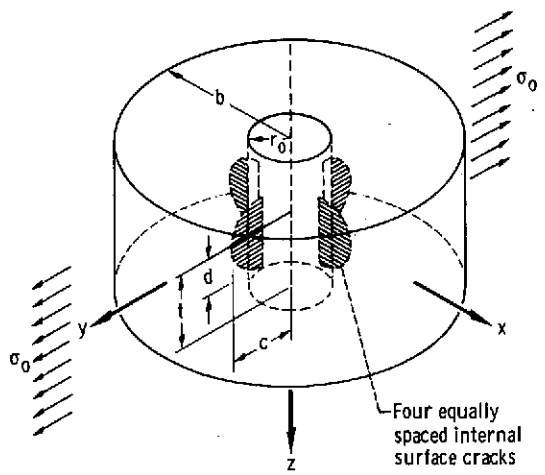

Figure 7. - Annular plate with internal surface cracks under uniform external tension.

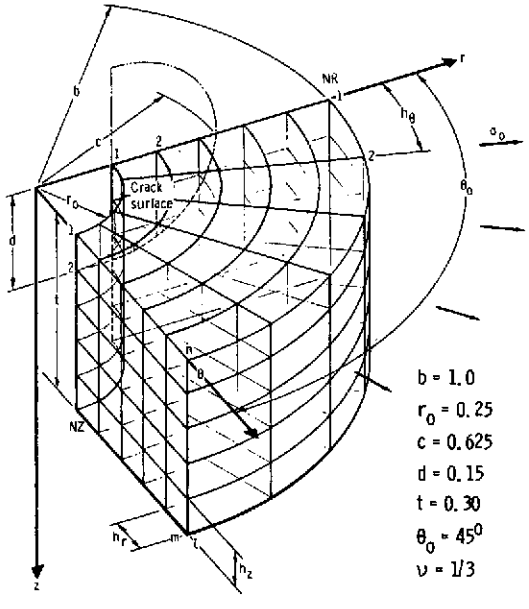

Figure 8. - Part of annular plate with internal surface cracks.

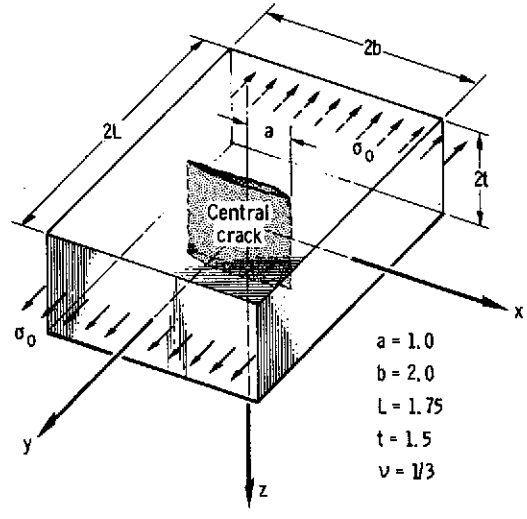

(a) Rectangular bar with through-thickness central crack.

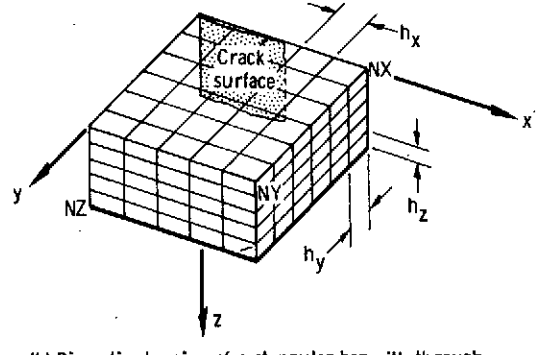

(b) Discretized region of rectangular bar with through-thickness central crack.

Figure 9. - Rectangular bar with through-thickness central crack under uniform tension.

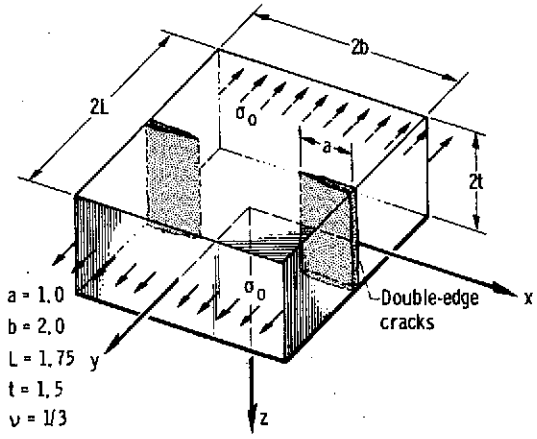

(a) Rectangular bar with through-thickness double edge cracks.

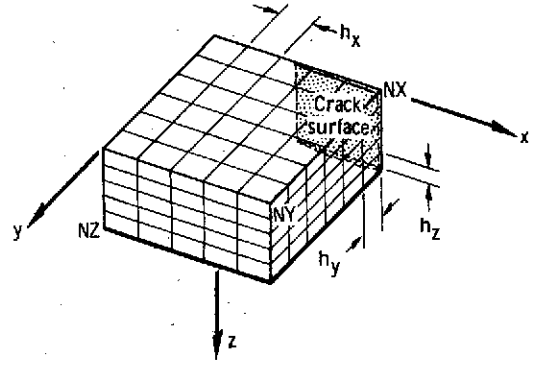

(b) Discretized region of rectangular bar with double-edge cracks.

Figure 10. - Rectangular bar with through-thickness double-edge cracks under uniform tension.

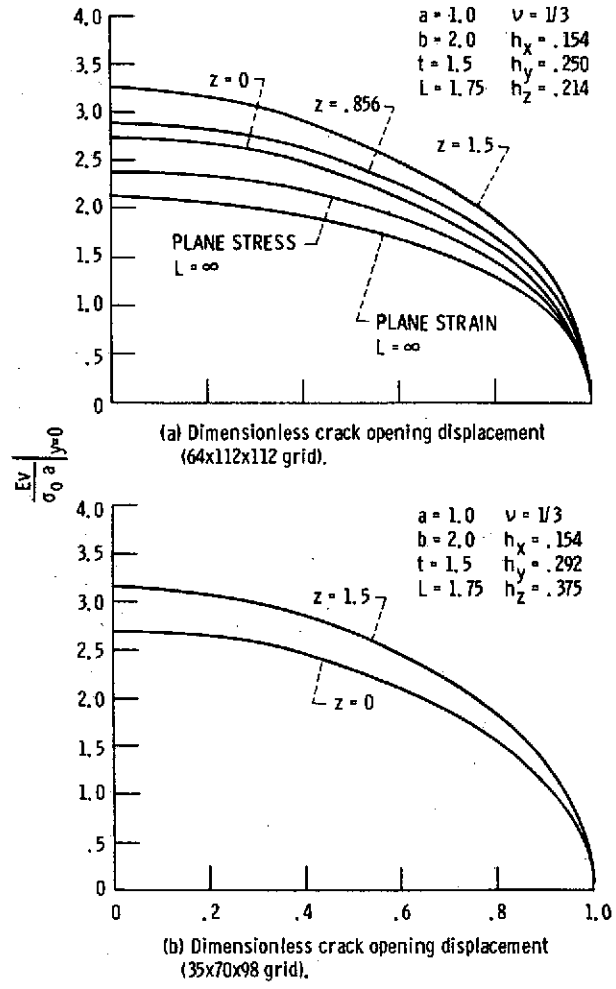

(a) Dimensionless crack opening displacement (64x112x112 grid).

(b) Dimensionless crack opening displacement (35x70x98 grid).

Figure 11. - Dimensionless crack opening displacement for a rectangular bar under uniform tension containing a through-thickness central crack.

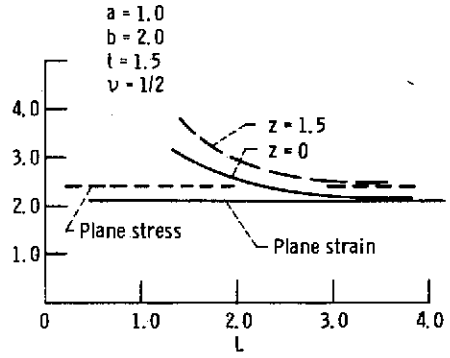

(c) Variation of crack opening displacement with bar length.

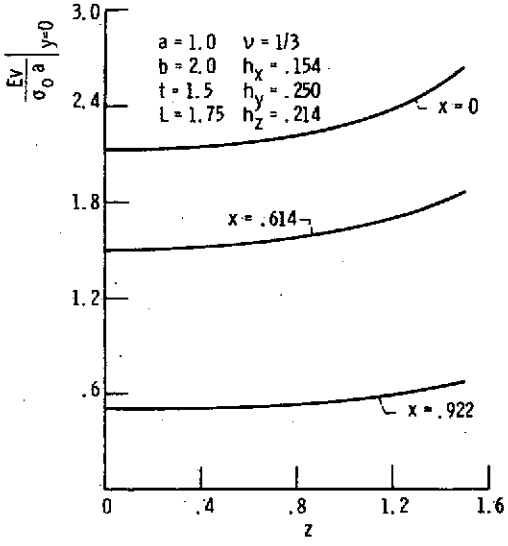

(d) Dimensionless crack opening displacement variation across bar thickness.

Figure 11. - Concluded.

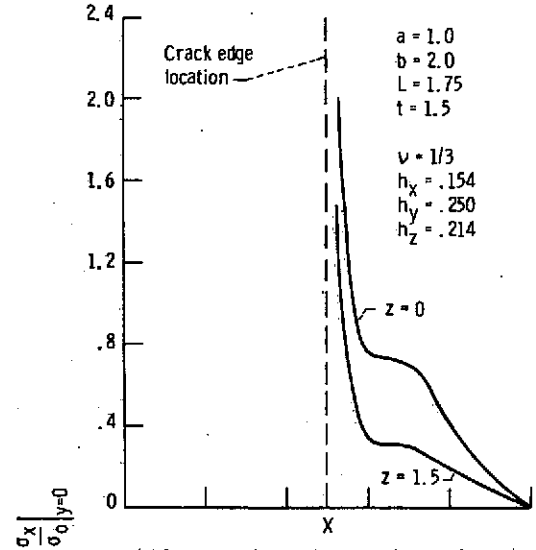

(a) Dimensionless x-directional normal stress variation along bar width.

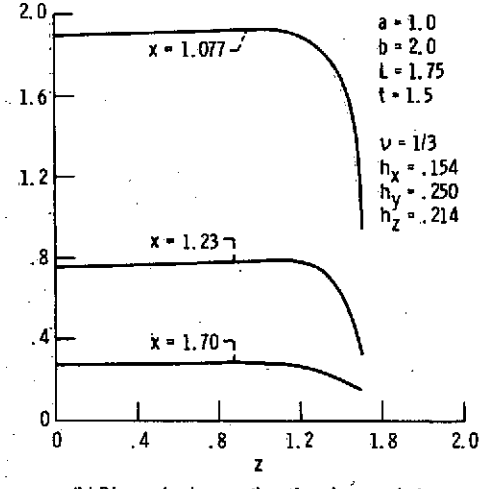

(b) Dimensionless x-directional normal stress variation across bar thickness.

Figure 12. - Dimensionless x-directional normal stress distribution in the crack plane for a rectangular bar under uniform tension containing a through-thickness central crack.

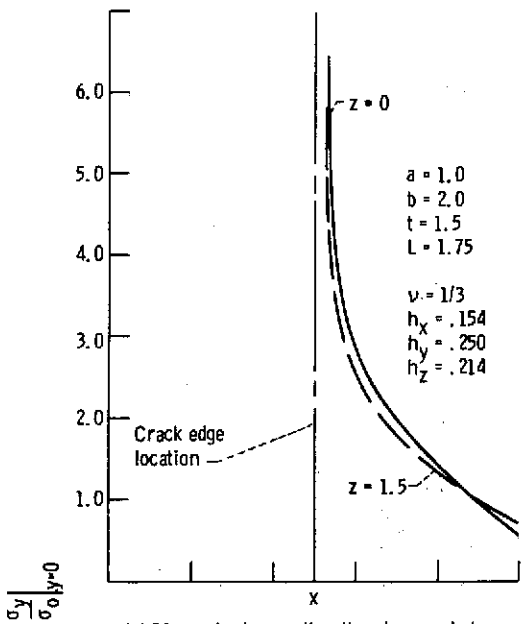

(a) Dimensionless y-directional normal stress variation along bar width.

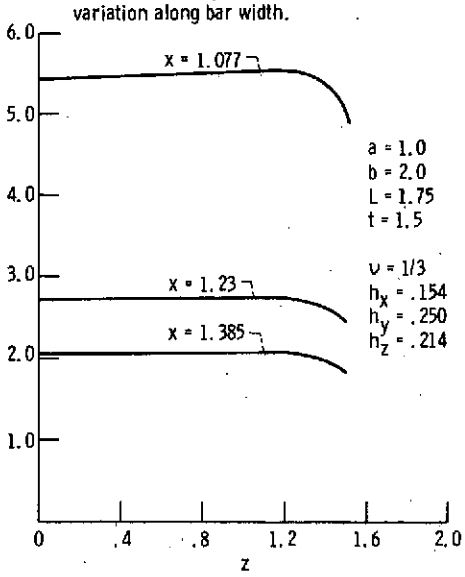

(b) Dimensionless y-directional normal stress variation across bar thickness.

Figure 13. - Dimensionless y-directional normal stress distribution in the crack plane for a rectangular bar under uniform tension containing a through-thickness central crack.

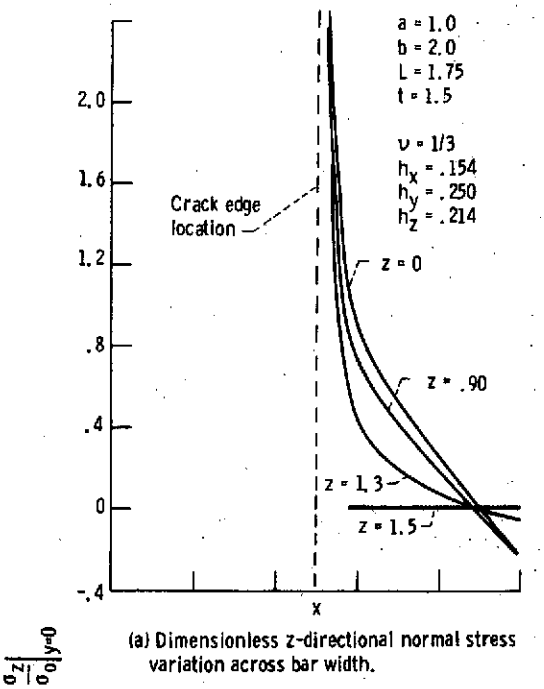

(a) Dimensionless z-directional normal stress variation across bar width.

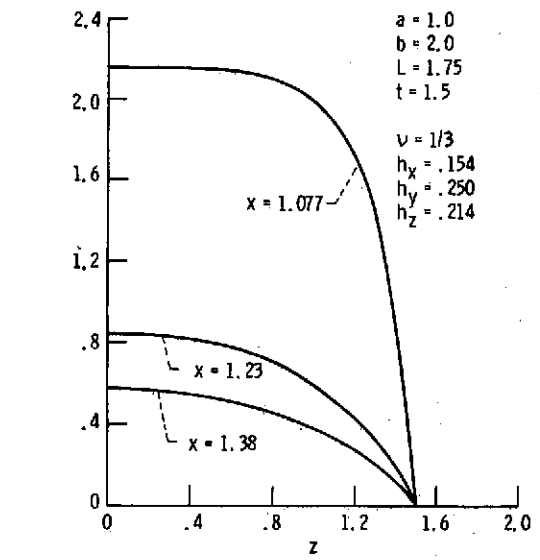

(b) Dimensionless z-directional normal stress variation across bar thickness.

Figure 14. - Dimensionless z-directional normal stress distribution in the crack plane for a rectangular bar under uniform tension containing a through-thickness central crack.

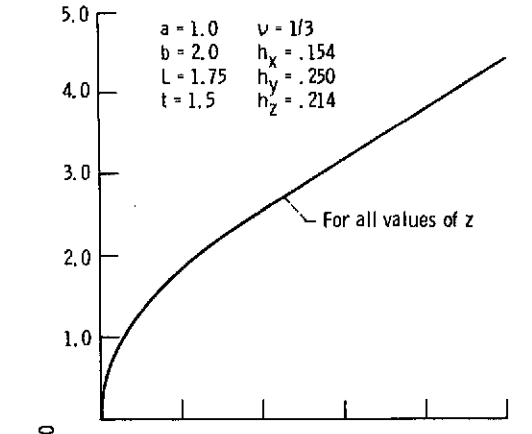

(a) Dimensionless crack opening displacement (64x112x112 grid).

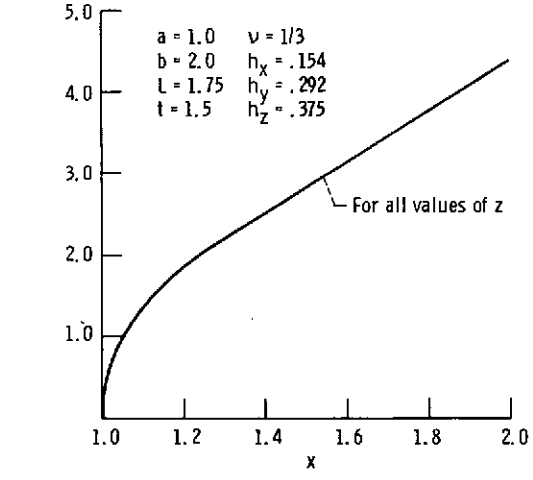

(b) Dimensionless crack opening displacement (35x70x98 grid).

Figure 15. - Dimensionless crack opening displacement for a rectangular bar under uniform tension containing through-thickness double edge cracks.

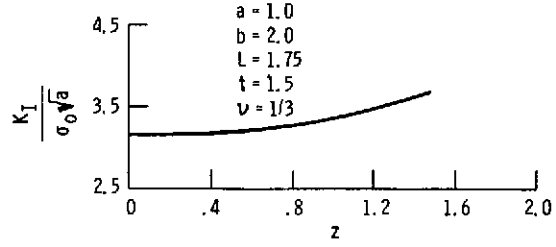

Figure 16. - Variation of stress intensity factor K_I across thickness for rectangular bar under uniform tension containing through-thickness central crack.